High-K negative parity states in ^{184}Os

T. Shizuma,[1] P. D. Stevenson,[2] P. M. Walker,[2] Y. Toh,[1] T. Hayakawa,[1] M. Oshima,[1] K. Furuno,[3] and T. Komatsubar[3]
[1]*Japan Atomic Energy Research Institute, Tokai, Ibaraki 319-1195, Japan*
[2]*Department of Physics, University of Surrey, Surrey GU2 7XH, United Kingdom*
[3]*Institute of Physics, University of Tsukuba, Ibaraki 305-8577, Japan*
(Received 15 January 2002; published 31 May 2002)

High-spin states in ^{184}Os have been studied using the ^{170}Er(^{18}O,4n) reaction at a beam energy of 85 MeV. Several new negative parity levels including a 48-ns $K^{\pi}=(18^{-})$ isomer have been identified. Nilsson configurations for the levels are assigned by comparison with multiquasiparticle calculations. Potential-energy-surface calculations show an increasing influence of triaxiality in nuclear shapes at higher spins. The decay rate of the $K^{\pi}=(18^{-})$ isomer is discussed in relation to the role of the K quantum number.

DOI: 10.1103/PhysRevC.65.064310 PACS number(s): 21.10.Re, 21.10.Tg, 23.20.Lv, 27.70.+q

I. INTRODUCTION

High-$K(=\Sigma_i\Omega_i)$ isomers in the Hf-W-Os nuclei with $A\approx 180$ arise due to the presence of many high-j and high-Ω orbitals near the Fermi surface [1]. For these axially deformed nuclei, the projection of the total angular momentum onto the nuclear symmetry axis K is approximately conserved. Consequently, the K selection rule governs the decay of the K isomers so that transitions from high-K to low-K bands are strongly hindered. These transitions, in practice, can proceed by admixture of K values. In rotating nuclei, the Coriolis interaction changes the spin orientation to lead to a $\Delta K=\pm 1$ mixing. On the other hand, shape fluctuations towards γ deformation can couple states with K quantum numbers differing by two units ($\Delta K=\pm 2$ mixing). In this context, of special interest have been the surprisingly low hindrances for the very large ΔK transitions [2–4]. So far, different mechanisms including Fermi-aligned Coriolis K mixing [3,5–7], γ tunneling through the potential barrier [2,4,8,9], and the statistical K mixing due to high level density [10] have been proposed for these transitions.

The hindrance factors per degree of K forbiddenness in the decay of highly excited K isomers in the heavier osmium ($Z=76$) isotopes [2,11,12] are typically much smaller than those observed in the hafnium isomers ($Z=72$) [13]. With the increased number of protons, the nuclear shapes become softer towards γ distortion. Furthermore, it is reported that the triaxial shapes appear at high spins in ^{184,186}Os [14,15]. Therefore, the γ-deformation degree of freedom, which introduces a substantial K mixing as stated above, is expected to play an important role in the reduction of the K conservation in the heavier osmium nuclei.

Prior to the present study, a 20-ns $K^{\pi}=10^{+}$ isomer was known in ^{184}Os [2]. A recent study also revealed detailed level structure especially for high-spin positive parity states in this nucleus [14]. Although there are predictions [14] that negative parity intrinsic states based on multiquasiparticle excitations are near the yrast line, less experimental evidence is available for such states. In this paper, we report on new negative parity states including $K^{\pi}=9^{-}$ and (13^{-}) bands, a 48-ns four-quasiparticle high-K isomer, and higher-seniority states.

II. EXPERIMENTS

High-spin states in ^{184}Os have been populated in the ^{170}Er(^{18}O,4n) reaction at a beam energy of 85 MeV. A 2.0 mg/cm^2 ^{170}Er target enriched to 95.88% with a 10 mg/cm^2 lead backing was bombarded by an ^{18}O dc beam derived from the 12UD tandem accelerator at University of Tsukuba. The target was thick enough to stop recoiling residuals. The beam energy was optimized for production of ^{184}Os ($4n$ exit channel) and ^{183}Os ($5n$ exit channel). Nine Compton-suppressed HP-Ge detectors, placed at 37° (two detectors), 79° (2), 101° (2), and 143° (3) with respect to the beam axis, were used to detect in-beam γ rays. In addition, one LEP detector at the angle of 79° was employed to increase detection efficiency for low-energy photons. A total of 2×10^8 correlated γ-γ-time events within 200 ns were collected. A complementary data set was obtained at the Japan Atomic Energy Research Institute (JAERI). The same reaction described above was used. 12 Compton suppressed HP-Ge detectors placed at angles of 32° (two detectors), 58° (2), 90° (4), 122° (2), and 148° (2) were used to collect approximately 1×10^8 γ-γ coincidence events. Both the data were separately sorted into two-dimensional γ-γ matrices. For analysis of isomers, γ-γ matrices with different time conditions were also created.

In order to determine transition multipole orders (dipole or quadrupole), DCO (directional angular correlation from oriented states) ratios [16,17] were extracted from the TSUKUBA data set. Here, the ratios are defined as

$$R_{\mathrm{DCO}}=\frac{I_\gamma \text{ at } 37^\circ \text{ (or } 143^\circ\text{) gated on } \gamma_G \text{ at } 79^\circ \text{ (or } 101^\circ\text{)}}{I_\gamma \text{ at } 79^\circ \text{ (or } 101^\circ\text{) gated on } \gamma_G \text{ at } 37^\circ \text{ (or } 143^\circ\text{)}}.$$

Since the angle of 101° (143°) is equivalent to that of 79° (37°) [17], the corresponding events can be summed when the DCO matrices are created. In the DCO analysis, stretched $\Delta I=2$ transitions close in the level scheme to the γ ray of interest are generally used as gates. In this case, the DCO ratios fall close to unity for stretched quadrupole ($\Delta I=2$) and unstretched dipole ($\Delta I=0$) transitions, and $R_{\mathrm{DCO}}\sim 0.6$ for stretched dipole ($\Delta I=1$) transitions. For mixed $\Delta I=1$ transitions, the DCO ratios depend on the mixing ratio δ.

 ©2002 The American Physical Society

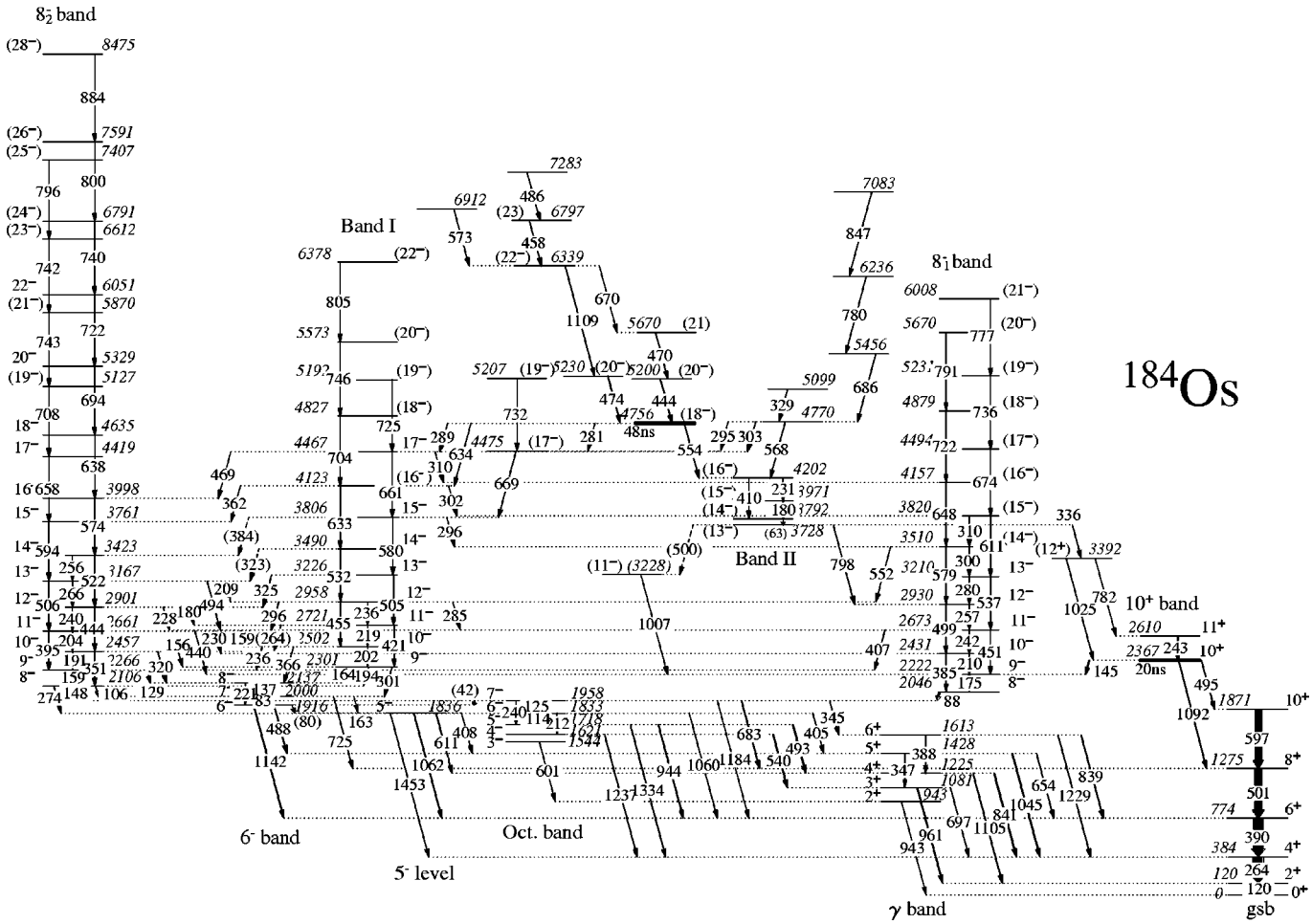

FIG. 1. A partial level scheme for ^{184}Os, showing the $K^\pi=5^-$ level and the γ-, octupole, $K^\pi=6^-$, 8_1^-, and 8_2^- bands, and bands I, II. Levels concerning the $K^\pi=(18^-)$ isomer are also shown.

III. RESULTS

Since a detailed study of ^{184}Os has recently been published [14], here the focus is on additional negative parity states that we found. Figure 1 shows the proposed partial level scheme resulting from the present work. Newly observed bands are labeled as band I and band II instead of the deduced K values. Note that the placement of 180, 231, 421, 580, 661, and 669 keV transitions are different from that of Ref. [14]. The ground state band, and the $K^\pi=10^+$ band based on the $\nu\{9/2^+[624]11/2^+[615]\}$ two-quasiparticle configuration were known up to high spins [2,14,18], but only the lower-spin members concerning the decay of a new isomer observed in this work are shown. The levels in γ octupole bands $K^\pi=5^-$ and 6^- two-quasiparticle states were also previously known [2,14]. The two $K^\pi=8^-$ bands based on the $\nu\{9/2^+[624]7/2^-[503]\}$ (8_1^- band) and $\nu\{9/2^+[624]7/2^-[514]\}$ (8_2^- band) two-quasiparticle configurations are confirmed and extended to higher spins from those reported in the previous work [14]. Table I summarizes energies, intensities, and DCO ratios for the γ-ray transitions in ^{184}Os shown in the level scheme (Fig. 1).

A. Band I

Three γ rays (164, 194, and 301 keV) have newly been found to deexcite a 2301 keV level into the $K^\pi=8_2^-$ and 6^- bands. The DCO ratio ($R_{\rm DCO}=0.34\pm0.03$) for the 194 keV transition is consistent with a $\Delta I=1$ radiation. In addition, based on the γ-ray intensity balance, a total conversion coefficient of the 194 keV transition was obtained as $\alpha_T=0.65\pm0.10$, which agrees with an $M1$ multipole [$\alpha_T^{\rm cal}(M1)=0.88$, $\alpha_T^{\rm cal}(E1)=0.07$]. The 2301 keV state, therefore, is confirmed as a $K^\pi=9^-$ state. A rotational band (band I) built on this state has been observed. Weak $\Delta I=1$ transitions connect the two signature sequences at lower spins. The spin assignment for the higher-lying levels is based on the DCO ratios, and confirmed by interband transitions from and into the $K^\pi=6^-$, 8_1^-, and 8_2^- bands.

B. New isomer at 4756 keV

From the analysis of delayed coincidence spectra, a new isomer has been observed at $E_x=4756$ keV, feeding the $I=16$ and 17 levels of band I by 634 and 289 keV transitions [Fig. 2(a)]. A sequence of 281 and 669 keV transitions via a 4475 keV $I^\pi=(17^-)$ level confirms the placement of the

TABLE I. Energies, level assignments, relative intensities, DCO ratios, and multipole assignments for the γ-ray transitions in ^{184}Os shown in Fig. 1.

E_γ [a] (keV)	E_i (keV)	J_i^π	$\rightarrow$	J_f^π	I_γ	R_{DCO}	ΔI
(42)	1958.3	7^-	$\rightarrow$	6^-			
(63)	3791.5	(14^-)	$\rightarrow$	(13^-)			
(80)	1916.4	6^-	$\rightarrow$	5^-			
83.3	2000.1	7^-	$\rightarrow$	6^-	4(1)		
88.2	2046.5	8^-	$\rightarrow$	7^-	16(1)	0.63(4)	1
106.3	2106.4	8^-	$\rightarrow$	7^-	3(2)	0.68(11)	1
114.4	1832.7	6^-	$\rightarrow$	5^-	12(1)	0.53(4)	1
119.7	119.7	2^+	$\rightarrow$	0^+	367(10)	1.00(1)	2
125.5	1958.3	7^-	$\rightarrow$	6^-	43(1)	0.48(2)	1
129.4	2266.1	9^-	$\rightarrow$	8^-	18(1)	0.66(3)	1
136.6	2136.7	8^-	$\rightarrow$	7^-	18(1)	0.63(6)	1
144.9	2366.8	10^+	$\rightarrow$	9^-	71(2)	0.57(6)	1
148.1	2106.4	8^-	$\rightarrow$	7^-	2(1)	0.40(9)	1
156.3	2457.0	10^-	$\rightarrow$	9^-	2(1)		
158.8	2661.3	11^-	$\rightarrow$	10^-	<1		
159.4	2266.1	9^-	$\rightarrow$	8^-	9(1)	0.76(8)	1
163.4	2000.1	7^-	$\rightarrow$	5^-	4(1)		
164.3	2300.7	9^-	$\rightarrow$	8^-	5(1)		
175.0	2221.6	9^-	$\rightarrow$	8^-	98(3)	0.55(6)	1
179.7	2901.0	12^-	$\rightarrow$	11^-	<1		
179.7	3971.2	(15^-)	$\rightarrow$	(14^-)	42(2)	0.50(5)	1
190.7	2457.0	10^-	$\rightarrow$	9^-	30(1)	0.81(6)	1
194.4	2300.7	9^-	$\rightarrow$	8^-	15(1)	0.34(3)	1
201.8	2502.5	10^-	$\rightarrow$	9^-	<1		
204.3	2661.3	11^-	$\rightarrow$	10^-	18(1)	0.58(4)	1
209.2	3166.8	13^-	$\rightarrow$	12^-	<1		
209.6	2431.2	10^-	$\rightarrow$	9^-	50(2)	0.33(3)	1
212.0	1832.7	6^-	$\rightarrow$	4^-	51(2)		
218.8	2721.3	11^-	$\rightarrow$	10^-	<1		
220.5	2136.7	8^-	$\rightarrow$	6^-	9(1)		
228.4	2901.0	12^-	$\rightarrow$	11^-	13(1)		
230.2	2661.3	11^-	$\rightarrow$	10^-	17(1)		
230.8	4202.1	(16^-)	$\rightarrow$	(15^-)	42(2)	0.61(3)	1
236.3	2957.6	12^-	$\rightarrow$	11^-	<1		
236.4	2502.5	10^-	$\rightarrow$	9^-	16(1)	0.71(5)	1
239.6	2901.0	12^-	$\rightarrow$	11^-	10(1)		
240.4	1958.3	7^-	$\rightarrow$	5^-	35(2)		
241.5	2672.8	11^-	$\rightarrow$	10^-	23(1)	0.21(3)	1
243.0	2609.8	11^+	$\rightarrow$	10^+	109(3)	0.42(1)	1
256.4	3423.2	14^-	$\rightarrow$	13^-	6(1)		
257.4	2930.3	12^-	$\rightarrow$	11^-	12(1)		
263.9	383.6	4^+	$\rightarrow$	2^+	990(30)		
(264)	2721.3	11^-	$\rightarrow$	10^-			
265.8	3166.8	13^-	$\rightarrow$	12^-	26(1)		
273.6	2106.4	8^-	$\rightarrow$	6^-	8(1)		
279.6	3209.9	13^-	$\rightarrow$	12^-	16(1)		
280.9	4756.1	(18^-)	$\rightarrow$	(17^-)	3(1)		
284.9	2957.6	12^-	$\rightarrow$	11^-	5(1)		
289.1	4756.1	(18^-)	$\rightarrow$	17^-	10(1)		
294.9	4770.0		$\rightarrow$	(17^-)	3(1)		
296.4	2957.6	12^-	$\rightarrow$	11^-	14(1)	0.42(4)	1
296.5	3806.3	15^-	$\rightarrow$	(14^-)	1(1)		

TABLE I. (*Continued*.)

E_γ [a] (keV)	E_i (keV)	J_i^π	→	J_f^π	I_γ	R_{DCO}	ΔI
299.8	3509.8	(14^-)	→	13^-	8(1)		
300.5	2300.7	9^-	→	7^-	10(1)		
302.1	4122.5	(16^-)	→	(15^-)	4(1)		
302.9	4770.0		→	17^-	9(1)		
309.6	4467.0	17^-	→	(16^-)	4(1)		
310.3	3820.5	(15^-)	→	(14^-)	8(1)		
320.2	2457.0	10^-	→	8^-	16(1)		
(323)	3489.6	14^-	→	13^-			
325.1	3226.1	13^-	→	12^-	7(1)		
329.5	5099.5				8(1)		
336.2	3728.2	(13^-)	→	(12^+)	14(1)	0.74(5)	1
345.2	1958.3	7^-	→	6^+	18(1)		
347.3	1428.2	5^+	→	3^+	4(1)		
350.8	2457.0	10^-	→	8^-	47(2)	0.96(2)	2
361.7	4122.5	(16^-)	→	15^-	5(1)		
365.8	2502.5	10^-	→	8^-	11(1)	1.10(8)	2
(384)	3806.3	15^-	→	14^-			
384.9	2431.2	10^-	→	8^-	9(1)		
388.0	1613.0	6^+	→	4^+	<1		
390.4	773.9	6^+	→	4^+	1000(30)	0.97(1)	2
395.1	2661.3	11^-	→	9^-	39(1)	0.93(2)	2
404.6	1832.7	6^-	→	5^+	16(1)		
406.7	2672.8	11^-	→	9^-	17(1)		
408.1	1836.3	5^-	→	5^+	2(1)		
410.1	4202.1	(16^-)	→	(14^-)	15(5)		
420.8	2721.3	11^-	→	9^-	25(1)	0.92(7)	2
439.8	2661.3	11^-	→	9^-	12(1)		
444.1	2901.0	12^-	→	10^-	48(2)	1.12(6)	2
451.0	2672.8	11^-	→	9^-	6(1)		
455.2	2957.6	12^-	→	10^-	17(1)		
469.3	4467.0	17^-	→	16^-	4(1)		
488.1	1916.4	6^-	→	5^+	50(2)		
493.1	1718.0	5^-	→	4^+	88(3)	0.73(2)	1
493.9	3166.8	13^-	→	11^-	13(1)		
495.4	2366.8	10^+	→	10^+	25(1)		
499.2	2930.3	12^-	→	10^-	15(1)		
(500)	3728.2	(13^-)	→	(11^-)			
500.8	1274.7	8^+	→	6^+	788(24)	1.01(1)	2
505.0	3226.1	13^-	→	11^-	30(1)	1.07(5)	2
505.6	3166.8	13^-	→	11^-	50(2)	1.00(5)	2
522.1	3423.2	14^-	→	12^-	51(2)	0.95(5)	2
532.0	3489.6	14^-	→	12^-	19(1)	0.96(6)	2
537.2	3209.9	13^-	→	11^-	18(1)		
539.9	1620.7	4^-	→	3^+	70(2)		
552.2	3509.8	(14^-)	→	12^-	<1		
554.0	4756.1	(18^-)	→	(16^-)	20(1)	1.11(17)	2
567.9	4770.0		→	(16^-)	14(1)		
574.5	3997.7	16^-	→	14^-	43(2)	1.17(6)	2
579.5	3509.8	(14^-)	→	12^-	17(1)		
580.3	3806.3	15^-	→	13^-	33(1)	0.90(5)	2
594.2	3760.9	15^-	→	13^-	51(2)	1.00(5)	2
596.7	1871.2	10^+	→	8^+	641(19)	1.02(1)	2
601.0	1544.0	3^-	→	2^+	<1		

TABLE I. (*Continued*.)

E_γ [a] (keV)	E_i (keV)	J_i^π	→	J_f^π	I_γ	R_{DCO}	ΔI
610.7	3820.5	(15^-)	→	13^-	28(1)		
611.4	1836.3	5^-	→	4^+	46(2)		
633.0	4122.5	(16^-)	→	14^-	32(1)		
634.4	4756.1	(18^-)	→	(16^-)	2(1)		
637.7	4635.4	18^-	→	16^-	34(1)	1.02(4)	2
647.6	4157.3	(16^-)	→	(14^-)	18(1)		
654.3	1428.2	5^+	→	6^+	22(1)		
657.8	4418.6	17^-	→	15^-	26(1)	0.90(5)	2
660.8	4467.0	17^-	→	15^-	19(1)	1.02(9)	2
669.2	4475.3	(17^-)	→	15^-	15(1)	0.92(9)	2
673.8	4494.2	(17^-)	→	(15^-)	13(1)		
683.5	1958.3	7^-	→	8^+	45(2)	0.80(2)	1
685.9	5455.9				13(1)		
694.0	5329.3	20^-	→	18^-	30(1)	0.90(4)	2
697.2	1080.9	3^+	→	4^+	14(1)		
704.2	4826.7	(18^-)	→	(16^-)	15(1)		
708.1	5126.7	(19^-)	→	17^-	23(1)	1.12(6)	2
721.6	6051.0	22^-	→	20^-	17(1)	1.16(6)	2
721.8	4879.2	(18^-)	→	(16^-)	5(1)		
725.4	5192.3	(19^-)	→	17^-	<1		
725.5	2000.1	7^-	→	8^+	19(1)	0.77(2)	1
732.2	5207.5	(19^-)	→	(17^-)	5(1)		
736.3	5230.5	(19^-)	→	(17^-)	10(1)		
739.9	6790.9	(24^-)	→	22^-	11(1)		
742.0	6611.7	(23^-)	→	(21^-)	8(1)		
743.0	5869.6	(21^-)	→	(19^-)	10(1)		
746.2	5572.8	(20^-)	→	(18^-)	9(1)		
777.1	6007.6	(21^-)	→	(19^-)	4(1)		
779.9	6235.8				8(1)		
782.2	3392.0	(12^+)	→	11^+	4(1)		
791.0	5670.2	(20^-)	→	(18^-)	5(1)		
795.7	7407.3	(25^-)	→	(23^-)	4(1)		
797.8	3728.2	(13^-)	→	12^-	13(1)	0.15(2)	1
800.0	7590.9	(26^-)	→	(24^-)	5(1)		
805.0	6377.8	(22^-)	→	(20^-)	5(1)		
839.0	1613.0	6^+	→	6^+	39(2)	0.84(1) [b]	0
841.5	1225.0	4^+	→	4^+	81(3)	0.84(1) [b]	0
847.3	7083.1				9(1)		
884.0	8474.9	(28^-)	→	(26^-)	3(2)		
943.0	943.0	2^+	→	0^+	<1		
944.1	1718.0	5^-	→	6^+	51(2)	0.87(2)	1
961.4	1080.9	3^+	→	2^+	69(3)	1.03(4)	1
1006.5	(3228)	(11^-)	→	9^-	5(1)		
1025.3	3392.0	(12^+)	→	10^+	13(1)	1.09(7)	2
1044.6	1428.2	5^+	→	4^+	74(3)	0.75(2)	1
1059.6	1832.7	6^-	→	6^+	7(1)		
1062.4	1836.3	5^-	→	6^+	49(2)	0.72(2)	1
1092.1	2366.8	10^+	→	8^+	38(1)	1.00(3)	2
1105.2	1225.0	4^+	→	2^+	39(2)	1.00(6)	2
1142.2	1916.4	6^-	→	6^+	62(2)	1.07(3)	0
1184.2	1958.3	7^-	→	6^+	5(1)		

TABLE I. (*Continued.*)

E_γ [a] (keV)	E_i (keV)	J_i^π	→	J_f^π	I_γ	$R_{\rm DCO}$	ΔI
1229.3	1613.0	6^+	→	4^+	26(1)	1.02(4)	2
1237.0	1620.7	4^-	→	4^+	26(1)	1.22(4)	0
1334.3	1718.0	5^-	→	4^+	33(1)	0.60(2)	1
1452.5	1836.3	5^-	→	4^+	15(1)	0.69(3)	1
Above the $I^\pi=(18^-)$ isomer							
443.6(1)	5199.6	(20^-)	→	(18^-)	39(2)	1.05(7)	2
457.7(1)	6797.1	(23)	→	(22^-)	15(1)	0.65(4)	1
470.2(1)	5669.8	(21)	→	(20^-)	20(1)	0.81(4)	1
473.9(1)	5230.1	(20^-)	→	(18^-)	41(2)	0.98(6)	2
486.1	7283.1				5(1)		
572.9	6912.3				8(1)		
669.7	6339.4	(22^-)	→	(21)	5(1)	0.70(5)	1
1109.3	6339.4	(22^-)	→	(20^-)	23(1)	1.09(5)	2

[a]The uncertainties of the transition energies are ±0.2 keV. Unobserved or uncertain transitions are put into parentheses.
[b]Doublet transitions.

isomeric level. As discussed in Sec. III C, the spin and parity of (18^-) are assigned for the isomer. Above this isomer, several transitions have been observed as seen in Fig. 2(c).

For determination of the half-life of the isomer, γ-ray time difference spectra (Fig. 3) between the transitions above and below the isomer have been analyzed. By fitting the decay slope, $T_{1/2}=48\pm5$ ns has been obtained for the isomer. The levels above the isomer have no measurable half-lives. We, therefore, took $T_{1/2}\leqslant3$ ns for these levels, as a limit of the present detection system.

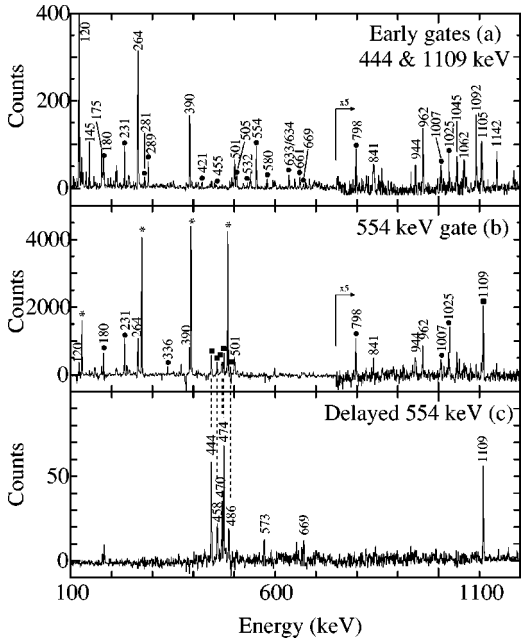

FIG. 2. Coincidence spectra gated on (a) the early 444 and 1109 keV transitions showing the transitions below the $K^\pi=(18^-)$ isomer, (b) the 554 keV transition, and (c) the delayed 554 keV transition, showing the transitions above the isomer. In panels (a) and (b), filled circles show the new transitions observed in the isomeric decay, filled squares show the transitions above the isomer, and asterisks denote contaminant transitions from ^{182}Os.

C. Band II

The 4756 keV isomer also decays into a 4202 keV level by a 554 keV transition. This transition is in coincidence with 180, 231, 336, 798, 1007, and 1025 keV transitions seen in Fig. 2(b), populating new levels at 4202, 3971, 3792, 3728, 3392, and 3228 keV. The placement of the 4202 keV level is further confirmed by transitions depopulating a 4770 keV level, which feed the 4202, 4467, and 4475 keV levels. The 3792, 3971, and 4202 keV levels are connected by the 180 keV ($R_{\rm DCO}=0.50\pm0.05$), 231 keV ($R_{\rm DCO}=0.61\pm0.03$) $\Delta I=1$ cascade transitions, and a weak 410 keV cross-over transition.

The 3728 keV level decays into the $K^\pi=8_1^-$ and 10^+ bands by the 336, 798, 1007, and 1025 keV transitions. Based on the DCO ratios of the 336 keV ($R_{\rm DCO}=0.74\pm0.05$), 798 keV ($R_{\rm DCO}=0.15\pm0.02$), and 1025 keV ($R_{\rm DCO}=1.09\pm0.07$) transitions, the 3728 keV state is assigned $I^\pi=(13^-)$. The present coincidence data imply an

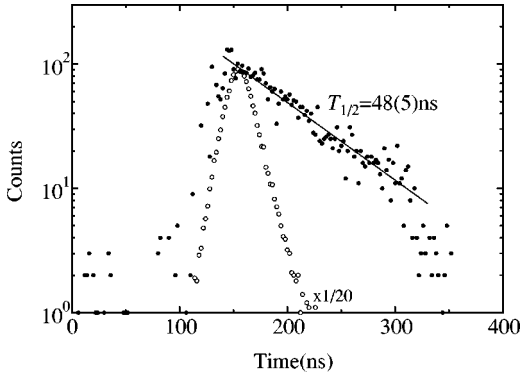

FIG. 3. A time difference spectrum between the 444, 474, 1109 keV transitions and the 554 keV transition, showing the decay curve for the $K^\pi=(18^-)$ isomer. The low intensity for time greater than 320 ns is due to the hard-wired gating conditions.

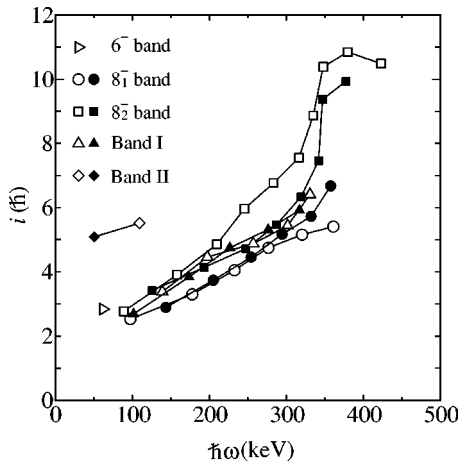

FIG. 4. Alignment plots for the negative parity bands observed in ^{184}Os. Harris parameters of $\Im_0 = 26$ MeV^{-1} $\hbar^2$ and $\Im_1 = 65$ MeV^{-3} $\hbar^4$ are taken from Ref. [14].

existence of a 63 keV transition connecting the 3728 and 3792 keV levels. This transition, however, cannot be separated from the intense $K_{\alpha 1}$ x-ray line in Os isotopes, and possibly has a large conversion factor. These preclude the observation of the 63 keV γ-ray line. Assuming that the unobserved 63 keV fast transition is of $M1$, $E1$, or $E2$ character, the 3792 keV level is assigned $I^\pi = (14^-)$, (14^+), or (15^-).

On the basis of the γ-ray intensity balances, $M1$ multipolarities are assigned for both the 180 keV [$\alpha_T^{\rm exp} = 1.3 \pm 0.2$, $\alpha_T^{\rm cal}(M1) = 1.1$] and 231 keV [$\alpha_T^{\rm exp} = 0.46 \pm 0.09$, $\alpha_T^{\rm cal}(M1) = 0.55$] transitions. Combining these with the DCO ratio of the 554 keV transition ($R_{\rm DCO} = 1.11 \pm 0.17$), the 4756 keV isomer is assigned $I^\pi = (18^-)$, (18^+), or (19^-). However, the $I^\pi = 18^+$ and 19^- assignments can be excluded since in these cases the 634 keV transition to the $I^\pi = (16^-)$ state in band I are of $M2$ or $M3$ character, and the transition strength for such higher multipoles is normally very weak. Consequently, we assigned $I^\pi = (14^-)$, (15^-), (16^-), and (18^-) for the 3792, 3971, 4202, and 4756 keV states, respectively.

IV. DISCUSSION

A. Rotational alignments

The magnitude of rotational alignments for multiquasiparticle bands depend on the alignments of constituent quasiparticles in the configuration, e.g., for bands which involve $i_{13/2}$ neutrons and/or $h_{9/2}$ protons, large rotational alignments are expected due to the strong Coriolis interaction on these quasiparticles (see, e.g., Ref. [19]). It can, therefore, be used to deduce quasiparticle configurations for rotational bands. In the cranked shell model [20] rotational alignments can be obtained by subtracting the aligned angular momentum of the reference configuration from the total aligned angular momentum $I_x [= \sqrt{I(I+1) - K^2}]$. In Fig. 4, the rotational alignments for the negative parity bands observed in ^{184}Os are shown as a function of the rotational frequencies $\hbar\omega$ given in units of keV. The Harris parameters used are $\Im_0 = 26$ MeV$^{-1}\hbar^2$ and $\Im_1 = 65$ MeV$^{-3}\hbar^4$ taken from Ref. [14]. In the calculation, we assume the K values fixed to the band-head spins (see also Sec. IV C).

The $K^\pi = 6^-$, 8_1^-, and 8_2^- bands show alignments of about $2\hbar$ consistent with the previous configuration assignments [14], including one aligned $i_{13/2}$ quasineutron. The alignment for band I is similar to those for the $K^\pi = 8_1^-$ and 8_2^- bands, indicating the presence of an $i_{13/2}$ quasineutron involved in the configuration. As discussed in Sec. IV C 2, a large alignment of $\sim 5\hbar$ for band II is due to the presence of three highly aligned $\nu i_{13/2}$ and $\pi h_{9/2}$ quasiparticles in the configuration.

B. g_K factors

Intensity ratios of $E2$ crossover to $M1(+E2)$ cascade transitions in a band can be used to deduce g_K factors within the rotational model [21]. Experimental $|g_K - g_R|$ values were obtained from the rotational expressions [19]. The values listed in Table II have been extracted with the assumption that K is equal to the band-head spin and the quadrupole moment of $Q_0 = 5.67$ e b taken from Ref. [2].

The calculated g_K factors [22] can be obtained in the semiclassical model [23] by the equation

$$g_K^{\rm eff} - g_R = \frac{\sum_j (g_{K_j} - g_R) K_j}{K} - \frac{\sum_j (g_{K_j} - g_R) i_j}{\sqrt{I^2 - K^2}}, \qquad (1)$$

where g_{K_j} is the gyromagnetic factor of the jth quasiparticle, i_j the aligned angular momentum, K_j the angular momentum projection on the deformation axis, and $K = \Sigma_j K_j$. The first term represents the usual expression of $(g_K - g_R)$ in the strong coupling limit, while the second term is due to the Coriolis effects which are important for configurations involving $i_{13/2}$ neutrons and/or $h_{9/2}$ protons in the present case. The i_j values were taken from the known one-quasiparticle bands of the neighboring odd-A nuclei. The g_{K_j} factors for each quasiparticle have been calculated from the equation of $g_{Kj} = (\langle l_3 \rangle g_l + \langle s_3 \rangle g_s)/K_j$, assuming 70% of the free nucleon g_s factors [24] ($g_s^{\rm free} = 5.59$ for protons and -3.83 for neutrons). Here, l_3 (s_3) is the projected component of the orbital angular momentum (intrinsic spin) on the nuclear symmetry axis, and $g_l = 1$ for protons, $g_l = 0$ for neutrons. The expectation values of s_3 were obtained from Nilsson wave functions. Table III summarizes the g_{K_j} factors and the alignments i_j used in the calculation.

The experimental and calculated $(g_K - g_R)$ values are compared in Table II. The deviations between the experimental and calculated values for the $K^\pi = 8_1^-$ and 8_2^- bands were attributed [14] to the configuration mixing of the two $K^\pi = 8^-$ configurations, $\nu\{7/2^-[503]\ 9/2^+[624]\}$ and $\nu\{7/2^-[514]\ 9/2^+[624]\}$. The g_K factors for bands I and II will be discussed below.

C. Configuration assignments

Wheldon *et al.* [14] have calculated the energies of multiquasiparticle states in ^{184}Os using the blocked BCS theory

TABLE II. g_K values deduced from the branching ratios for the negative parity bands in ^{184}Os.

Band	I_i	$E_\gamma(E2)$ (keV)	$E_\gamma(M1/E2)$ (keV)	λ	$\lvert g_K^{\rm exp}-g_R\rvert$[a]	$(g_K^{\rm cal}-g_R)$[b]
6^-	8	221	137	0.52(3)	0.10(2)	−0.29
8_1^-	10	385	210	0.18(2)	0.32(2)	−0.42
	11	451	242	0.25(4)	0.43(1)	−0.45
	12	499	257	1.3(1)	0.24(1)	−0.48
	13	537	280	1.1(1)	0.31(1)	−0.49
	(14)	579	300	2.1(2)	0.25(1)	−0.50
	(15)	611	310	3.7(3)	0.20(1)	−0.51
8_2^-	10	351	191	1.6(1)	0.02(2)	−0.15
	11	395	204	2.2(1)	0.10(1)	−0.19
	12	444	240	4.9(3)	0.04(1)	−0.21
	13	506	266	1.9(1)	0.20(1)	−0.23
	14	522	256	8.2(5)	0.10(1)	−0.24
Band I	12	455	236	3.3(3)	0.04(2)	−0.27
Band II	(16)	410	231	0.35(12)	0.15(3)	−0.14

[a] $Q_0 = 5.67\ e$ b [2] is used.
[b] The calculated values have uncertainties of ±0.05 propagated from the assumption of $g_R = 0.32 \pm 0.05$ [2].

described in Ref. [25]. The calculations compare well with the observed excitation energies for the positive parity four- and six-quasiparticle states. In the following, Nilsson configurations for the negative parity states are discussed in comparison with the multiquasiparticle calculations.

1. Band I

The band-head spin and parity for band I are $K^\pi = 9^-$. A favored $K^\pi = 9^-$ state with $\nu\{7/2^-[514]\ 11/2^+[615]\}$ is predicted at 2385 keV close to the $I^\pi = 9^-$ state of band I (2301 keV). The alignment of about $2\hbar$ extracted for this band (see Fig. 4) supports the above configuration that involves an aligned $i_{13/2}$ neutron. However, the experimental small $\lvert g_K - g_R\rvert$ value of 0.04 ± 0.02 is not consistent with the predicted value of $(g_K^{\rm cal} - g_R) = -0.27$ for the proposed configuration. A plausible explanation is that this is due to mixing with a $K^\pi = 8^- \pi\{5/2^+[402]11/2^-[505]\}$ two-quasiparticle proton band which is predicted [14] at 2490 keV near the $K^\pi = 9^-$ state. Since the large positive value of $g_K^{\rm cal}(=1.3)$ is expected for the $K^\pi = 8^- \pi\{5/2^+[402]11/2^-[505]\}$ band, about 20 % mixing into the $K^\pi = 9^-$ band would be enough to reproduced the weak $\Delta I = 1$ transitions.

TABLE III. g_{K_j} factors and alignments of the single-particle orbitals considered for ^{184}Os.

Neutrons	g_{K_j}	i_j	Protons	g_{K_j}	i_j
$1/2^-[521]$	0.64	0.0	$1/2^-[541]$	0.76	3.5
$1/2^-[510]$	−1.50	0.0	$5/2^+[402]$	1.57	0.0
$7/2^-[514]$	0.26	0.0	$9/2^-[514]$	1.30	0.5
$7/2^-[503]$	−0.34	0.0	$11/2^-[505]$	1.24	0.5
$9/2^+[624]$	−0.23	2.0			
$11/2^+[615]$	−0.18	1.0			

2. Band II

The spins and parities for the 3728 and 3792 keV states connected by the unobserved 63 keV transition were assigned as (13^-) and (14^-) in Sec. III C. Since the upper limit of the half-life ($T_{1/2} \leqslant 3$ ns) for the 3792 keV level is not conclusive for proving its intrinsic or collective character, possible configurations with $K^\pi = 13^-$ or 14^- states are discussed below.

In the multiquasiparticle calculations [14], the $K^\pi = 13^-$ state with a four-quasiparticle configuration of $\nu\{9/2^+[624]11/2^+[615]\} \otimes \pi\{1/2^-[541]5/2^+[402]\}$ is predicted at $E_x^{\rm cal} = 3556$ keV, while no low-lying $K^\pi = 14^-$ state is expected in ^{184}Os. Furthermore, the observed $(g_K^{\rm exp} - g_R)$ value of $\pm(0.15 \pm 0.03)$ agrees with the $K^\pi = 13^-$ configuration $[(g_K^{\rm cal} - g_R) = -0.14]$. Consequently, we assign the $K^\pi = 13^- \nu\{9/2^+[624]11/2^+[615]\} \otimes \pi\{1/2^-[541]5/2^+[402]\}$ configuration for band II built on the 3728 keV state. The compressed first rotational transition (63 keV) is possibly due to Coriolis effects of the aligned $1/2^-[541]$ proton involved in the proposed configuration. This phenomenon is observed for the bands with similar configurations in ^{178}W [26], ^{179}W [19], and ^{183}Os [12]. The large alignment of $i \sim 5\hbar$ as shown in Fig. 4 also support the $K^\pi = 13^-$ configuration including aligned $\nu i_{13/2}$ and $\pi h_{9/2}$ orbitals.

TABLE IV. Multiquasiparticle configurations for low-lying negative parity levels in ^{184}Os. Predictions ($E_x^{\rm cal}$) and the experimental $K^\pi=5^-$, 6^-, 8_1^-, and 8_2^- states are taken from Ref. [14].

K^π	Configurations	$E_x^{\rm cal}$ (keV)	$E_x^{\rm exp}$ (keV)
5^-	$\nu\{1/2^-[510]9/2^+[624]\}$	1900	1836
6^-	$\nu\{1/2^-[521]11/2^+[615]\}$	2101	1916
8_1^-	$\nu\{7/2^-[503]9/2^+[624]\}$	2008	2046
8_2^-	$\nu\{7/2^-[514]9/2^+[624]\}$	2426	2106
9^-	$\nu\{7/2^-[514]11/2^+[615]\}$	2385	2301
13^-	$\nu\{9/2^+[624]11/2^+[615]\}\pi\{1/2^-[541]5/2^+[402]\}$	3556	3728
18^-	$\nu\{9/2^+[624]11/2^+[615]\}\pi\{5/2^+[402]11/2^-[505]\}$	4407	4756
22^-	$\nu\{1/2^-[521]7/2^-[503]9/2^+[624]11/2^+[615]\}$ $\pi\{5/2^+[402]11/2^-[505]\}$	5757	(6339)
23^-	$\nu\{3/2^-[512]7/2^-[514]9/2^+[624]11/2^+[615]\}$ $\pi\{5/2^+[402]11/2^-[505]\}$	6278	(6797)
25^-	$\nu\{7/2^-[503]7/2^-[514]9/2^+[624]11/2^+[615]\}$ $\pi\{5/2^+[402]11/2^-[505]\}$	6168	
26^-	$\nu\{7/2^-[514]9/2^-[505]9/2^+[624]11/2^+[615]\}$ $\pi\{5/2^+[402]11/2^-[505]\}$	7205	
30^-	$\nu\{7/2^-[503]7/2^-[514]9/2^+[624]11/2^+[615]\}$ $\pi\{1/2^-[541]5/2^+[402]9/2^-[514]11/2^-[505]\}$	7898	

3. The $K^\pi=(18^-)$ isomer and the higher-lying levels

The 4756 keV isomer is assigned $K^\pi=(18^-)$ as discussed in Sec. III C. The most favored $K^\pi=18^-$ configuration is a $\nu\{9/2^+[624]11/2^+[615]\}\otimes\pi\{5/2^+[402]11/2^-[505]\}$ four-quasiparticle state predicted [14] at 4407 keV. The $K^\pi=(18^-)$ state having the same configuration has been observed at 5027 keV in ^{186}Os [15]. It would be noted that the differences between the calculated and observed excitation energies are close to each other, $\Delta E=E_x^{\rm cal}-E_x^{\rm exp}=-349$ keV for ^{184}Os and $\Delta E=-331$ keV for ^{186}Os.

Several levels are placed above the $K^\pi=(18^-)$ isomer, but no well-defined rotational structure can be seen. In the multiquasiparticle calculations [14], six-quasiparticle states of $K^\pi=22^-$ $\nu\{1/2^-[521]7/2^-[503]9/2^+[624]11/2^+[615]\}\otimes\pi\{5/2^+[402]11/2^-[505]\}$ at $E_x=5757$ keV and $K^\pi=23^-$ $\nu\{3/2^-[512]7/2^-[514]9/2^+[624]11/2^+[615]\}\otimes\pi\{5/2^+[402]11/2^-[505]\}$ at $E_x=6278$ keV are predicted as favored configurations. The $I^\pi=(22^-)$ state at $E_x=6339$ keV and the $I=(23)$ state at $E_x=6797$ keV could correspond to the predicted $K^\pi=22^-$ and 23^- states. The level structure will be further discussed in Sec. IV E in relation to triaxiality of nuclear shapes. The proposed configurations for the negative parity states in ^{184}Os are summarized in Table IV.

D. *K*-forbidden transitions

The 289, 554, and 634 keV transitions depopulating the $K^\pi=(18^-)$ isomer are K forbidden, i.e., the changes in the K quantum numbers are greater than the transition multipole orders $\Delta K>\lambda$. Table V summarizes the hindrance factors F and the hindrance factors per degree of K forbiddenness (or reduced hindrance factor) f_ν for the transitions depopulating the $K^\pi=(18^-)$ isomer in ^{184}Os. These factors are defined as $f_\nu=F^{1/\nu}=(T_{1/2}^\gamma/T_W)^{1/\nu}$ where $\nu(=\Delta K-\lambda)$ is the order of K forbiddenness, $T_{1/2}^\gamma$ and T_W are the partial γ-ray half-life and the corresponding Weisskopf single-particle estimate.

The f_ν values of 4.7, 3.7, and 8.2 for the 289, 634, and 554 keV transitions are smaller than the corresponding values observed in the $N=108$ isotone ^{182}W [27], i.e., $f_\nu=20$ and 14 for the 356 keV $M1$ and 676 keV $E2$ transitions from the $K^\pi=15^+$ four-quasiparticle isomer to the $K^\pi=10^+$ band. This is possibly due to the γ softness expected in the heavier osmium nuclei [2], or K mixing by high level density discussed below.

TABLE V. Hindrance factors for the K-forbidden transitions from the $K^\pi=(18^-)$ isomer observed in ^{184}Os.

K^π	E_γ (keV)	$K^{\rm final}$	$E_x^{\rm final}$ (keV)	$T_{1/2}^\gamma$ (ns)	ΔK	$L\lambda$ [a]	F	f_ν
(18^-)	281		4475	627		$M1$	6.3×10^5	
	289	9	4467	188	9	$M1$	2.0×10^5	4.7
	634	9	4123	940	9	$E2$	1.1×10^4	3.8
	554	(13)	4202	94	5	$E2$	5.5×10^2	8.2

[a]Assuming stretched $M1$ for the $\Delta I=1$ transitions and stretched $E2$ for the $\Delta I=2$ transitions in extraction of the total (conversion-corrected) intensities.

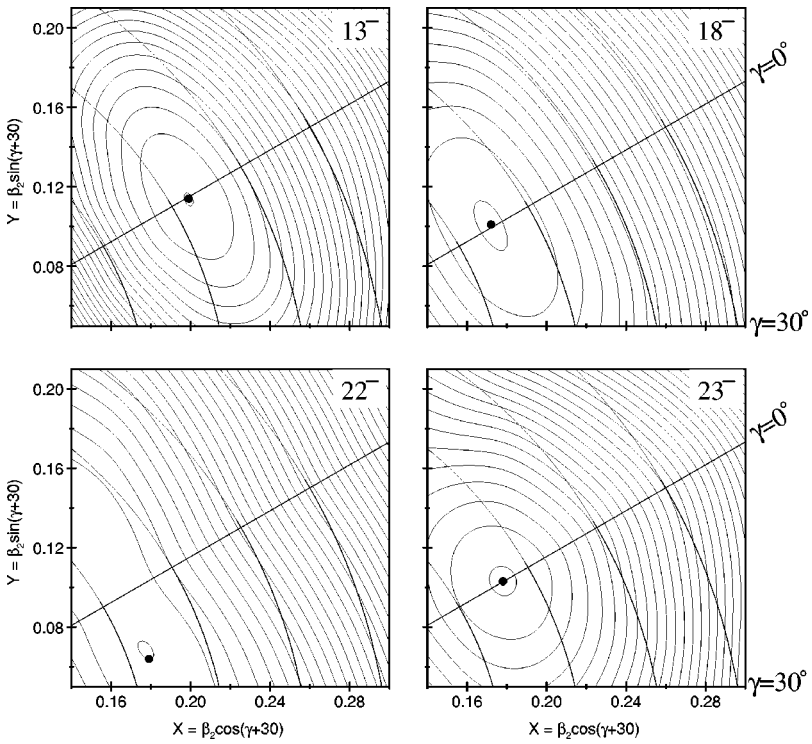

FIG. 5. Configuration-constrained potential-energy-surface calculations. Top left: the $K^{\pi}=13^{-}$ state, top right: the $K^{\pi}=18^{-}$ state, bottom left: the $K^{\pi}=22^{-}$ state, bottom right: the $K^{\pi}=23^{-}$ state (see also Table VI). The potentials are reflection symmetric about the $\gamma=0°$ axis.

Walker *et al.* have analyzed decay rates of high-K isomers in terms of statistical K mixing which depends on the density of states [10]. States with lower-K values are assumed to be mixed and introduce low-K components into the isomeric state. The systematics reveal a striking correlation between the f_{ν} values and the excitation energies of K isomers (E_K), relative to the energy of a rigid rotor [$E_R=(\hbar^2/2\Im)I(I+1)$ with the moment of inertia $\Im$ of a rigid rotor] in the K-forbidden transitions from four- to two-quasiparticle states. In the density-of-states estimate the f_{ν} value can be obtained as

$$f_{\nu}^{\mathrm{stat}}=F_{\nu}\exp\left[-\frac{3}{\nu}\sqrt{\frac{A}{7.5}(E_K-E_R)}\right], \tag{2}$$

where F_{ν} is a constant for a given value of ν and A is the mass number. The reduced hindrance factors decline depending on the relative excitation energies of the isomers. Using the same prescription as in Ref. [10], the hindrance factor for the $\Delta K=9$ $E2$ (634 keV) transition from the $K^{\pi}=(18^{-})$ isomer in ^{184}Os, is calculated as $f_{\nu}^{\mathrm{stat}}=4.6$ with $E_K-E_R=4.756-1.968=2.788$ MeV, which compares well with the observed f_{ν} value of 3.7. This result follows the systematic trend obtained in Ref. [10]. Since the rotational alignment of band I is blocked due to the occupation of an $i_{13/2}$ neutron orbital, the effects of K mixing in the populated states would be small. On the other hand, it was suggested that the lower value of $f_{\nu}^{\mathrm{exp}}=2.3$ observed for the ^{182}Os, $\Delta K=16$ $E2$ (1530 keV) transition with a similar E_K-E_R value of 2.794 MeV, results from the involvement of high-K, Fermi-aligned couplings in the populated states [10].

A number of four- and six-quasiparticle states have been observed in ^{184}Os. Among them, only the $K^{\pi}=(18^{-})$ isomer is relatively long lived ($T_{1/2}=48$ ns). This is a consequence of the details of the level structure of this nucleus. In the $I=13-18$ region, only the $K^{\pi}=(13^{-})$ and (18^{-}) intrinsic states are observed, and thus the $K^{\pi}=(18^{-})$ isomer can only decay by K-forbidden transitions with $\Delta K\geqslant 5$.

E. Potential-energy-surface calculations

Configuration-constrained potential-energy-surface (PES) calculations were performed for the positive parity states in ^{184}Os [14], where the nuclear potential was calculated using the Lipkin-Nogami formalism of pairing with a Woods-Saxon potential as described by Xu *et al.* [28]. While the ground state and the $K^{\pi}=10^{+}$ state have axially symmetric shapes ($\beta_2\approx 0.19$ and $|\gamma|\approx 0°$), the $K^{\pi}=21^{+}$ state is predicted to have a triaxial deformation with $\beta_2=0.20$ and $|\gamma|=11°$ [14].

In the present study, the shape evolution for the negative parity states in ^{184}Os has been investigated using the same configuration-constrained PES calculation code. As shown in Fig. 5, the $K^{\pi}=13^{-}$ and 18^{-} configurations, corresponding to the experimentally observed $E_x=3728$ and 4756 keV state, have axially symmetric shapes ($\beta_2=0.23$ and 0.20 with $|\gamma|\approx 0°$). On the other hand, the PES calculations predict that triaxially deformed states ($K^{\pi}=22^{-}$, 25^{-}, and 30^{-}) become increasingly favored at higher spins, competing with prolate deformed states ($K^{\pi}=23^{-}$ and 26^{-}) as shown in Table VI. Deformations for the $K^{\pi}=22^{-}$ and 23^{-} configurations, which could correspond to the observed $E_x=6339$ and 6797 keV states, are calculated to be $(\beta,|\gamma|)=(0.19,10°)$ and $(0.21,0°)$, respectively (Fig. 5). The occupation of the $7/2^{-}[503]$ neutron orbital forces the nucleus towards triaxial deformation [15]. The possible role of triaxiality has been discussed in connection with the short-

TABLE VI. Calculated deformations for the four-, six-, and eight-quasiparticle negative parity states in ^{184}Os.

K^π	β_2	β_4	$\lvert\gamma\rvert$
13^-	0.23	−0.043	0°
18^-	0.20	−0.050	0°
22^-	0.19	−0.040	10°
23^-	0.21	−0.065	0°
25^-	0.20	−0.038	6°
26^-	0.20	−0.032	0°
30^-	0.22	−0.026	6°

lived nature of the positive parity states in ^{184}Os [14] and ^{186}Os [15]. Although the triaxial shapes are predicted to appear at low energy for the negative parity states in ^{184}Os, the effect of the triaxiality on the level structure remains to be clarified due to lack of the experimental information. Further investigation is certainly needed.

V. SUMMARY

We have newly observed negative parity levels consisting of $K^\pi=9^-$ and (13^-) bands as well as a 48-ns $K^\pi=(18^-)$ isomer. The quasiparticle configurations for these states were assigned by comparison with multiquasiparticle calculations. The $K^\pi=(18^-)$ isomer decays with large K changes ($K \geqslant 5$), resulting in the relatively long half-life. However, the low hindrances (f_ν) for the isomeric transitions are interpreted as being due to K mixing from a combination of γ softness and high level density. Configuration-constrained PES calculations for the negative parity states in ^{184}Os show that the triaxially deformed states ($K^\pi=22^-$, 25^-, and 30^-) compete with the axially deformed states ($K^\pi=23^-$ and 26^-) at high spins. The 6339 keV state has been tentatively assigned as the $K^\pi=22^-$ triaxially deformed state. Further experimental investigation is required to reveal the role of triaxiality in K conservation.

ACKNOWLEDGMENTS

We would like to thank Dr. C. Wheldon for the discussion on the multiquasiparticle calculations, and Professor G. Sletten and J. Sørensen for the target preparation. The staff of the tandem accelerator center at University of Tsukuba and the JAERI tandem accelerator are also thanked for providing the ion beams.

[1] P. M. Walker and G. D. Dracoulis, Nature (London) **399**, 35 (1999).

[2] P. Chowdhury, G. D. Fabricius, C. Christensen, F. Azgui, S. Bjørnholm, J. Borggreen, A. Holm, J. Pedersen, G. Sletten, M. A. Bentley, D. Howe, A. R. Mokhtar, J. D. Morrison, J. F. Sharpey-Schafer, P. M. Walker, and R. M. Lieder, Nucl. Phys. **A485**, 136 (1988).

[3] P. M. Walker, G. Sletten, N. L. Gjørup, M. A. Bentley, J. Borggreen, B. Fabricius, A. Holm, D. Howe, J. Pedersen, J. W. Roberts, and J. F. Sharpey-Schafer, Phys. Rev. Lett. **65**, 416 (1990); N. L. Gjørup, P. M. Walker, G. Sletten, M. A. Bentley, B. Fabricius, and J. F. Sharpey-Schafer, Nucl. Phys. **A582**, 369 (1995).

[4] B. Crowell, P. Chowdhury, S. J. Freeman, C. J. Lister, M. P. Carpenter, R. G. Henry, R. V. F. Janssens, T. L. Khoo, T. Lauritsen, Y. Liang, F. Soramel, and I. G. Bearden, Phys. Rev. Lett. **72**, 1164 (1994); B. Crowell, P. Chowdhury, D. J. Blumenthal, S. J. Freeman, C. J. Lister, M. P. Carpenter, R. G. Henry, R. V. F. Janssens, T. L. Khoo, T. Lauritsen, Y. Liang, F. Soramel, and I. G. Bearden, Phys. Rev. C **53**, 1173 (1996).

[5] P. M. Walker, G. D. Dracoulis, A. P. Byrne, B. Fabricius, T. Kibèdi, and A. E. Stuchbery, Phys. Rev. Lett. **67**, 433 (1991).

[6] P. M. Walker, K. C. Yeung, G. D. Dracoulis, P. H. Regan, G. J. Lane, P. M. Davidson, and A. E. Stuchbery, Phys. Lett. B **309**, 17 (1993).

[7] S. Frauendorf, in *Proceedings of the International Conference on the Future of Nuclear Spectroscopy*, Crete, 1993, edited by W. Gelletly, C. A. Kalfas, R. Vlastou, S. Harissopulos, and D. Loukas (INP, National Center for Scientific Research Demokritos, Athens, 1994), p. 112.

[8] T. Bengtsson, R. A. Broglia, E. Vigezzi, F. Barranco, F. Dønau, and Jing-ye Zhang, Phys. Rev. Lett. **62**, 2448 (1989).

[9] K. Narimatsu, Y. R. Shimizu, and T. Shizuma, Nucl. Phys. **A601**, 69 (1996).

[10] P. M. Walker, D. M. Cullen, C. S. Purry, D. E. Appelbe, A. P. Byrne, G. D. Dracoulis, T. Kibèdi, F. G. Kondev, I. Y. Lee, A. O. Macchiavelli, A. T. Reed, P. H. Regan, and F. Xu, Phys. Lett. B **408**, 42 (1997).

[11] T. Kutsarova, R. M. Lieder, H. Schnare, G. Hebbinghaus, D. Balabanski, W. Gast, A. Krämer-Flecken, M. A. Bentley, P. Fallon, D. Howe, A. R. Mokhtar, J. F. Sharpey-Schafer, P. Walker, P. Chowdhury, B. Fabricius, G. Sletten, and S. Frauendorf, Nucl. Phys. **A587**, 111 (1995).

[12] T. Shizuma, K. Matsuura, Y. Toh, T. Hayakawa, M. Oshima, Y. Hatsukawa, M. Matsuda, K. Furuno, Y. Sasaki, T. Komatsubara, and Y. R. Shimizu, Nucl. Phys. **A696**, 337 (2001).

[13] P. M. Walker, Phys. Scr. **T5**, 29 (1983), and references therein.

[14] C. Wheldon, G. D. Dracoulis, R. T. Newman, P. M. Walker, C. J. Pearson, A. P. Byrne, A. M. Baxter, S. Bayer, T. Kibèdi, T. R. McGoram, S. M. Mullins, and F. R. Xu, Nucl. Phys. **A699**, 415 (2002).

[15] C. Wheldon, P. M. Walker, P. H. Regan, T. Saitoh, N. Hashimoto, G. Sletten, and F. R. Xu, Phys. Rev. C **59**, R2334 (1999); Nucl. Phys. **A652**, 103 (1999).

[16] K. S. Krane, R. M. Steffen, and R. M. Wheeler, Nucl. Data Tables **11**, 351 (1973).

[17] L. P. Ekström and A. Nordlund, Nucl. Instrum. Methods Phys. Res. A **313**, 421 (1992).

[18] T. Shizuma, K. Matsuura, T. Jumatsu, K. Hata, Y. Sasaki, H. Ishiyama, M. Kato, K. Uchiyama, T. Komatsubara, K. Furuno,

and T. Hayakawa Phys. Lett. B **442**, 53 (1998).
[19] P. M. Walker, G. D. Dracoulis, A. P. Byrne, B. Fabricius, T. Kibèdi, A. E. Stuchbery, and N. Rowley, Nucl. Phys. **A568**, 397 (1994).
[20] R. Bengtsson and S. Frauendorf, Nucl. Phys. **A327**, 139 (1979).
[21] A. Bohr and B. R. Mottelson, *Nuclear Structure* (Benjamin, Reading, MA, 1975), Vol. 2.
[22] R. A. Bark, G. B. Hagemann, B. Herskind, H. J. Jensen, W. Korten, J. Wrzesinski, H. Carlsson, M. Bergström, A. Brockstedt, A. Nordlund, H. Ryde, P. Bosetti, S. Leoni, F. Ingebretsen, and P. O. Tjøm, Nucl. Phys. **A591**, 265 (1995).
[23] F. Dönau and S. Frauendorf, in *Proceedings of the Conference on High Angular Momentum Properties of Nuclei*, Oak Ridge, Tennessee, 1982, edited by N. R. Johnson (Harwood Academic, New York, 1983), p. 143; F. Dönau, Nucl. Phys. **A471**, 469 (1987).
[24] H. Morinaga and T. Yamazaki, *In-beam Gamma-ray Spectroscopy* (North-Holland, Amsterdam, 1975)
[25] K. Jain, O. Burglin, G. D. Dracoulis, B. Fabricius, N. Rowley, and P. M. Walker, Nucl. Phys. **A591**, 61 (1995).
[26] C. S. Purry, P. M. Walker, G. D. Dracoulis, T. Kibèdi, F. G. Kondev, S. Bayer, A. M. Bruce, A. P. Byrne, W. Gelletly, P. H. Regan, C. Thwaites, O. Burglin, and N. Rowley, Nucl. Phys. **A632**, 229 (1998).
[27] P. H. Regan, P. M. Walker, G. D. Dracoulis, S. S. Anderssen, A. P. Byrne, P. M. Davidson, T. Kibèdi, G. J. Lane, A. E. Stuchbery, and K. C. Yeung, Nucl. Phys. **A567**, 414 (1994).
[28] F. R. Xu, P. M. Walker, J. A. Sheikh, and R. Wyss, Phys. Lett. B **435**, 257 (1998).